Monthly Notices
of the
ROYAL ASTRONOMICAL SOCIETY

MNRAS **497,** 1115–1126 (2020)
Advance Access publication 2020 July 10

doi:10.1093/mnras/staa2009

Swift/*XRT*, *Chandra*, and *XMM–Newton* observations of IGR J17091–3624 as it returns into quiescence

M. Pereyra [1★] D. Altamirano,[2] J. M. C. Court,[3] N. Degenaar,[4] R. Wijnands,[4] A. S. Parikh[4] and V. A. Cúneo [5,6]

[1]*CONACYT, Instituto de Astronomía, Universidad Nacional Autónoma de México, 22860 Ensenada, BC, Mexico*
[2]*School of Physics and Astronomy, University of Southampton, B46, Southampton SO17 1BJ, UK*
[3]*Department of Physics and Astronomy, Texas Tech University, PO Box 41051, Lubbock, TX 79409, USA*
[4]*Anton Pannekoek Institute for Astronomy, University of Amsterdam, Science Park 904, NL-1098 XH Amsterdam, the Netherlands*
[5]*Instituto de Astrofísica de Canarias (IAC), E-38205 La Laguna, Tenerife, Spain*
[6]*Departamento de Astrofísica, Universidad de La Laguna, E-38206 La Laguna, Tenerife, Spain*

Accepted 2020 July 1. Received 2020 June 30; in original form 2020 April 6

ABSTRACT

IGR J17091–3624 is a low-mass X-ray binary (LMXB), which received wide attention from the community thanks to its similarities with the bright black hole system GRS 1915+105. Both systems exhibit a wide range of highly structured X-ray variability during outburst, with time-scales from few seconds to tens of minutes, which make them unique in the study of mass accretion in LMXBs. In this work, we present a general overview into the long-term evolution of IGR J17091–3624, using *Swift*/*XRT* observations from the onset of the 2011–2013 outburst in 2011 February till the end of the last bright outburst in 2016 November. We found four re-flares during the decay of the 2011 outburst, but no similar re-flares appear to be present in the latter one. We studied, in detail, the period with the lowest flux observed in the last 10 yr, just at the tail end of the 2011–2013 outburst, using *Chandra* and *XMM-Newton* observations. We observed changes in flux as high as a factor of 10 during this period of relative quiescence, without strong evidence of softening in the spectra. This result suggests that the source has not been observed at its true quiescence so far. By comparing the spectral properties at low luminosities of IGR J17091–3624 and those observed for a well-studied population of LMXBs, we concluded that IGR J17091–3624 is most likely to host a black hole as a compact companion rather than a neutron star.

Key words: accretion, accretion discs – stars: low-mass – X-rays: binaries – X-rays: individual: IGR J17091–3624.

1 INTRODUCTION

Among the whole population of binary systems in the universe, low-mass X-ray binaries (LMXBs) are one of the best targets to study the accretion processes occurring in extreme physical regimes. These systems are formed by a low-mass star orbiting a compact object, which can be either a neutron star (NS) or a black hole (BH), that accretes matter from its low-mass stellar companion by Roche lobe overflow. Depending on the amount of mass transferred to the compact object, LMXBs will exhibit different accretion states during their lives. The extremes of these accretion regimes are the so-called outburst and quiescence states, characterized by high and low X-ray luminosity, respectively. During outburst, LMXBs have been observed at very high luminosities in the 0.5–10 keV band, within a range of 10^{34}–10^{39} erg s^{-1}. In the quiescent state, when very low or no mass accretion takes place, their luminosities are as low as 10^{30}–10^{33} erg s^{-1} (e.g. Remillard & McClintock 2006; Jonker, Bassa & Wachter 2007; Heinke et al. 2008; Plotkin, Gallo & Jonker 2013; Wijnands, Degenaar & Page 2013; Reynolds et al. 2014; Wijnands et al. 2015; and references therein). Although many observational properties of LMXBs at high luminosities are relatively well understood, given the current sensitivity of X-ray instruments, the spectral behaviour of LMXBs at luminosities $\lesssim 10^{34}$ erg s^{-1} is less clear (Wijnands & Degenaar 2013; Yang 2016; Christodoulou et al. 2018). GRS 1915+105 is one of the well-known LMXBs whose behaviour at the high-luminosity regime is fairly well characterized and extensively studied in an outburst (Belloni et al. 2000). Since the discovery of outburst in 1992 (Castro-Tirado, Brandt & Lundt 1992), an exponential decay of its X-ray emission has been observed a few times (Negoro et al. 2018). The source also exhibited an unusual low-flux state last year (Homan et al. 2019), with short X-ray and bright radio flares (Balakrishnan et al. 2019; Koljonen et al. 2019; Ridnaia et al. 2019; and references therein). More recently, evidence of renewed activity in the microquasar has been observed by *INTEGRAL* and *MAXI* instruments (Lepingwell et al. 2020; Aoki et al. 2020). GRS 1915+105 is a very peculiar BH binary that exhibits a complex X-ray variability in time-scales from few seconds to tens of minutes. Its X-ray light curve shows several quasi-periodic oscillations at high and low frequencies, often associated with the existence of instabilities in the accretion disc (e.g. Janiuk, Czerny & Siemiginowska 2000). Over the last decades, only two other LMXBs have exhibited some of the exotic variabilities observed in GRS 1915+105: the BH candidate IGR J17091–3624 and the NS MXB

★ E-mail: m.pereyra.astronomer@gmail.com

1730–335 (Altamirano et al. 2011; Bagnoli & in't Zand 2015; Maselli et al. 2018). Although both sources have experienced quiescent periods in the past, to characterize their behaviour in this state requires detailed observations at very low luminosities which had been only possible for IGR J17091–3624 (see e.g. Wijnands, Yang & Altamirano 2012).

IGR J17091–3624 has shown multiple outbursts from the time of its discovery in 2003 (Revnivtsev et al. 2003; Capitanio et al. 2006). For the last two of its outbursts, an extensive observing campaign was performed by the current X-ray missions. During these two outbursts at least nine variability classes were identified to resemble those previously seen in GRS 1915+105 (Altamirano et al. 2011; Capitanio et al. 2012; Pahari et al. 2013; Zhang et al. 2014; Court et al. 2017). The presence of extreme winds in the accretion disc, similar to those observed in GRS 1915+105, associated to its quasi-periodic variability, has also been reported (by King et al. 2012; Janiuk et al. 2015). The transient nature of IGR J17091–3624 allowed X-ray missions to also observed it at very low count rates, in the so called quiet periods. The first quiet period was observed by *XMM–Newton* in 2006 and 2007, with only two observations performed at that time, as reported by Wijnands et al. (2012). For the second quiet period, at the very tail end of the 2011 outburst, five observations were performed by *Chandra* and *XMM–Newton* instruments at different epochs. Additionally, *Swift/XRT* observations provided a very nice coverage of its transition from outburst to quiescence, making the source particularly interesting to study the low-level accretion in X-ray binaries.

Although it is well known that a large number of LMXBs spend most of their life in a dormant state, with very weak or zero mass accretion, the definition of this quiescent state in BH binaries is still a matter of debate. To define an upper limit for low-accretion regimes, parameters like the normalized Eddington X-ray luminosity l_x (with $l_x = L_x/L_{Edd}$, where L_x is the X-ray luminosity from 0.5 to 10 keV and $L_{Edd} = 1.26 \times 10^{38}\ (M/M_\odot)\ erg\ s^{-1}$ for ionized hydrogen) are commonly used (Remillard & McClintock 2006; Plotkin et al. 2013). Under these assumptions, a $10\,M_\odot$ BH with $l_x \sim 10^{-8.5}-10^{-5.5}$, corresponding to $L_x \sim 10^{30.5}-10^{33.5}\ erg\ s^{-1}$, is considered to be in a quiescent state. The low X-ray flux observed in this regime has been generally associated to radiatively inefficient accretion flows (RIAFs; see Narayan & Yi 1994; Narayan & McClintock 2008; and references therein) and the observed correlation between the X-ray flux and the presence of radio jets proposed by Fender, Gallo & Jonker (2003), Gallo et al. (2006), and Miller-Jones et al. (2008) has also become an interesting scheme to explain the spectral properties of X-ray binaries in quiescence (Miller-Jones et al. 2011; Plotkin et al. 2016). The conditions under which they reach the true quiescent state are not well understood either. Re-flaring activity or mini-outburst episodes have been widely detected in many LMXBs, with different time-scales and brightness, but very little is know about the physical mechanisms that generate them (see e.g. Lasota 2001; Patruno et al. 2009; Patruno et al. 2016; Parikh & Wijnands 2017). To analyse how the quiescent stage is influenced by the transition from outburst to quiet periods, requires a detailed characterization of the long term variability like the one presented here. We have studied the X-ray emission of IGR J17091–3624, outside the outburst regime, by following its transition towards quiescence. We characterized the long-term X-ray variability observed in the source after the main outburst in 2011 and analysed the spectral properties at the lowest luminosity period observed over the last decade. Finally, we pointed out the differences observed in the X-ray properties of the source during its last two outbursts and discuss the implications of our results in the context of previous findings for this source and other LMXBs.

2 OBSERVATIONS

To characterize the time evolution of IGR J17091–3624 X-ray flux during its last two outbursts, we used data obtained with the *Swift/XRT* instrument (Burrows et al. 2000), on board of the Neil Gehrels *Swift* Observatory (Gehrels et al. 2004), performed between 2011 February (MJD 55595) and 2016 November (MJD 57690). To study the transition of the source towards quiescence, we selected archived *Chandra* (Weisskopf 1999) and *XMM–Newton* (Barré, Nye & Janin 1999) observations performed within June–October of 2013. These data, presented here for the first time, correspond to the last five months of the 2011–2013 outburst (for further information about the behaviour of the source in outburst we refer to Grinberg et al. 2016; Court et al. 2017; Xu et al. 2017; Radhika et al. 2018; Gatuzz et al. 2020; and references therein).

2.1 *Swift*

2.1.1 *Light curve*

We retrieved the X-ray light curve from *Swift* observations using the *Swift/XRT* data products generator (see Evans et al. 2007, 2009). Considering a snapshot binning method (a single and continuous on-target exposure of 300–2700 s), we extracted a 0.3–10 keV long term light curve from MJD 55500 to 58200, which includes the outburst onset in 2011 February (MJD 55595) and the last *Swift/XRT* observations of IGR J17091–3624 in 2018 (MJD 58151). In the light curve presented in Fig. 1, black circles correspond to detections above 3σ. Upper limits are marked with black arrows, usually associated to observations at low count rates with short exposure times ($\leq$400 s).

2.1.2 XRT *spectra*

The data were downloaded from the HEASARC archive and processed using the XRTPIPELINE tool. We extracted the spectra using XSELECT. A source region of 40 arcsec centred on the source location was used. An annular background region (also centred on the source location) having an inner radius of 150 arcsec and an outer radius of 250 arcsec was used. The ancillary response files were created using the XRTMKARF tool and the appropriate response matrix files, as suggested by the tool, were used. The spectra were binned to have a minimum number of 10 counts per bin for data taken in the Window Timing (WT) mode and 2 counts per bin for data taken in the Photon Counting (PC) mode.

2.2 *XMM–Newton*

2.2.1 *EPIC spectra*

The data were acquired with the *European Photon Imaging Camera (EPIC)* using the *MOS* and *pn* CDD arrays in full frame configuration and the thin optical blocking filter (Turner et al. 2001; Strüder et al. 2001). We used a 33.7 ks observation performed on 2013 September 12 (MJD 56547). Observation IDs (OBSIDs), energy range, and count rates used for each camera are presented in Table 1. To obtain the event files lists, we reprocessed the Original Data Files (ODFs) using EPPROC task from *XMM–Newton* SAS (Science Analysis System) v.1.2, adopting standard procedures.[1] Due to high-energy particle background events detected at the end of the observation, we excluded the last 10 ks from the *EPIC/pn* data and 4 ks from

[1] https://www.cosmos.esa.int/web/xmm-newton/sas-threads

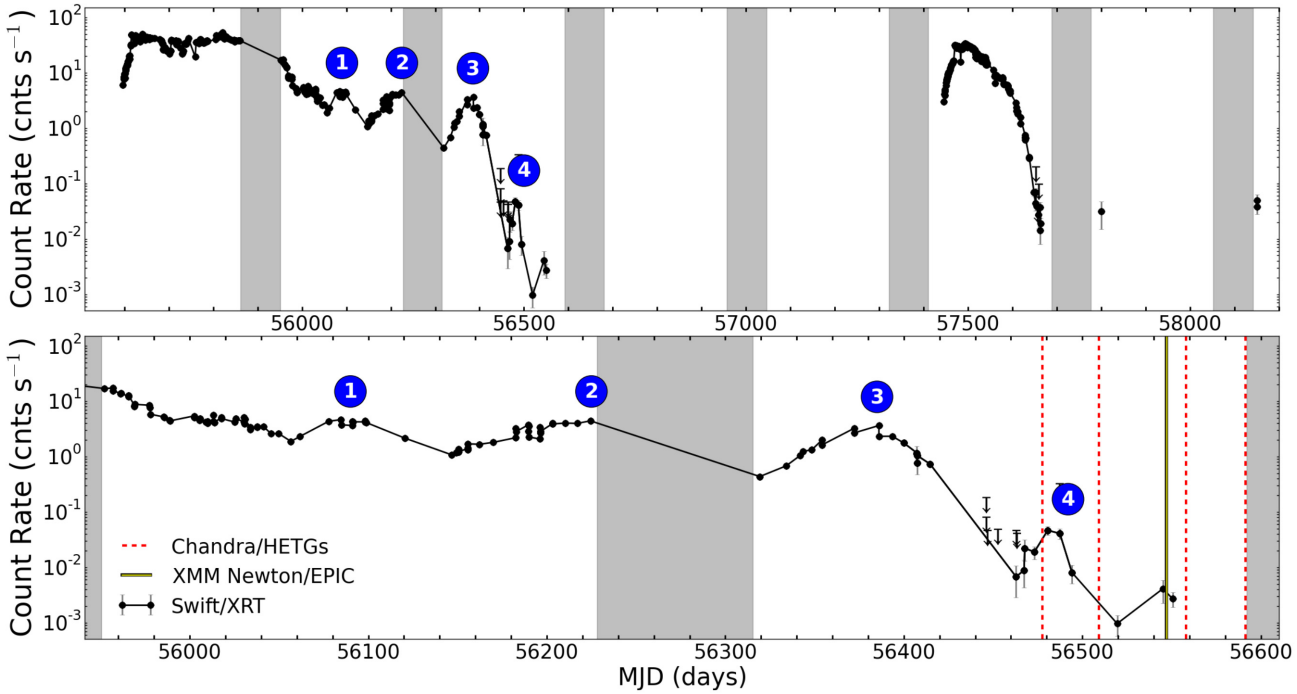

Figure 1. Top panel: *Swift/XRT* long-term light curve of IGR J17091–3624 in the 0.3–10 keV band, showing the last two outbursts experienced by the source in 2011 February (MJD 55595) and 2016 February (MJD 57445). Bottom panel: Zoom in on the re-flaring period of the source observed at the tail end of the 2011 outburst. Four different re-flares are clearly seen, the peaks are marked with blue circles. Black arrows indicate *Swift/XRT* 3σ upper limits. Gray shaded areas correspond to the times when the source was not observed by *Swift/XRT* due to Sun constraints. The dashed red and solid yellow vertical lines in the bottom panel indicate the times when *Chandra* and *XMM–Newton* observations were performed, respectively. Please refer to Sections 4.1 and 4.2 for a detailed description of this figure.

Table 1. Log of the *Chandra* and *XMM–Newton* observations.

OBS ID	Date (DD/MM/YYY)	Exposure time (ks)	Telescope Instrument	Energy range (keV)	Count rate (10^{-3} counts s^{-1})	Total number of counts
			Chandra			
14658	04/07/2013	39.3	*ACIS/HETGS*(HEG)	0.8–10	9.1 ± 0.5	394
			ACIS/HETGS(MEG)	0.4–5	11.1 ± 0.1	467
			ACIS/HETGS(Zeroth)	0.4–10	29 ± 1	1132
14659	05/08/2013	40.5	*ACIS/HETGS*(HEG)	0.8–10	0.5 ± 0.2	30
			ACIS/HETGS(MEG)	0.4–5	1.5 ± 0.3	85
			ACIS/HETGS(Zeroth)	0.4–10	2.9 ± 0.3	125
14660	23/09/2013	42.2	*ACIS/HETGS*(HEG)	0.8–10	0.9 ± 0.2	56
			ACIS/HETGS(MEG)	0.4–5	2.8 ± 0.3	138
			ACIS/HETGS(Zeroth)	0.4–10	3.0 ± 0.3	138
14661	26/10/2013	39.2	*ACIS/HETGS*(HEG)	0.8–10	2.4 ± 0.3	136
			ACIS/HETGS(MEG)	0.4–5	3.1 ± 0.4	156
			ACIS/HETGS(Zeroth)	0.4–10	7.2 ± 0.4	296
			XMM–Newton			
		33.7	*EPIC(pn)*	0.2–15	23.9 ± 0.8	807
0721200101	12/09/2013	39.8	*EPIC(MOS1)*	0.2–15	6.1 ± 0.5	346
		39.2	*EPIC(MOS2)*	0.2–15	6.9 ± 0.5	405

those of the *MOS* cameras. The source spectrum was extracted with *XMMSELECT* using a circular region of 25 arcsec centred on the source. To estimate the background contribution we used a 50 arcsec annulus region around the source position, with an inner radius of 30 arcsec, excluding the source extraction region. Redistribution matrix and ancillary files were created using *RMFGEN* and ARFGEN, respectively. All the spectra were grouped to contain at least 15 counts per bin. Due to the very low count rates at the time of the observation, data from the *Reflecting Grating Spectrometer* were not considered for this analysis.

2.3 *Chandra*

We retrieved four observations from the *Chandra* data archive. The data were acquired with the *Advanced CCD Imaging Spectrometer S-array* (*ACIS-S*; Garmire et al. 2003) operating in a Faint Timed Exposure mode, and the *High Energy Transmission Gratings (HETGS)* in the focal plane with the zeroth-order flux incident in the S3 chip. The *HETGS* on board of *Chandra* consists of two sets of gratings: the Medium Energy Grating (MEG) and the High Energy Gratings (HEG), optimized for medium energies and high energies, respectively. We created event files using CHANDRA_REPRO script from CIAO (*Chandra* Interactive Analysis of Observations) 4.8 and the CALDB (Calibration Data Base) 4.7.0 software, following standard analysis threads.[2] Energy ranges and final count rates for each spectrum are described in Table 1.

2.3.1 *HETGS zeroth-order spectra*

To extract zeroth-order grating spectra, we used SPECTEXTRACT CIAO tool, following standard procedures.[3] We used a circular spatial region of 6.5, centered in the zeroth-order location automatically selected by TGDETECT in the CHANDRA_REPRO script, to obtain the source spectrum. The ancillary and response files were generated by *SPECEXTRACT* during spectra extraction. All the spectra were grouped to contain at least 15 counts per bin.

2.3.2 *HETGS first-order spectra*

We extracted pha2 files for both gratings using TGEXTRACT2[4] CIAO tool. The REGION block of the pha2 file was used to extract the source dispersed flux. We estimated the background considering an extraction region of the same size of that used for the source. The background flux was estimated from the events with cross-dispersion contained in the regions lying above and below the source extraction region. The source and background first-order spectra from the HEG and MEG, as well as their corresponding redistribution matrix and ancillary files, were obtained using TGSPLIT and MKTGRESP, respectively. To increase the signal-to-noise ratio of the extracted spectra, we combined the −1 and +1 orders for each arm using COMBINE_GRATING_SPECTRA.

3 DATA ANALYSIS

The spectral fitting was conducted with XSPEC v.12.9.0 (Arnaud 1996). We used χ^2 statistics to fit *Swift/XRT, EPIC,* and *HETGS* zeroth-order spectra. When HETGS first-order spectra and *Swift/XRT* spectra with the lowest count rates (2 counts/bin) were considered, we used *cash* statistics.

Only for the *EPIC* data, the highest quality data, it was possible to analyse five different emission models that are commonly used to describe LMXBs spectra: a power-law photon spectrum (POWERLAW), thermal bremsstrahlung (BREMSS), blackbody radiation (BBODY), accretion disc/multi-blackbody emission (DISKBB), and an NS hydrogen atmosphere model (NSATMOS). We included the effect of neutral hydrogen absorption $N_{\rm H}$ using the TBABS model version 1.0 with default XSPEC abundances (Wilms, Allen & McCray 2000) and cross-sections (Verner et al. 1996). To give the reader an idea of the quality of our data at the lowest count rates, the best fit for *EPIC/pn* spectra is presented in Fig. 2 compared to previous studies data at similar count rates (Wijnands et al. 2012). The X-ray flux was calculated considering different energy ranges, according to the instruments responses, using the convolution model CFLUX. Since the distance to the source is unknown, to estimate its luminosity we considered distances commonly used in previous works, which place the source between 8 and 35 kpc. The errors reported here are at a 90 per cent confidence level unless otherwise stated. In the following sections, we present a detailed description of the spectral analysis performed for each data set individually.

3.1 *Swift/XRT* data

From the light curve presented in Fig. 1, we see that there is a remarkable difference in the flux level of *Swift/XRT* data along the transition period, from outburst to quiescence, that have to be considered carefully. Although we confirmed that for the highest count rates was feasible to use two-component models (BBODY + POWERLAW) to fit the data, this was not necessarily the case for those data sets with the lowest count rates. By using the same models to fit both types of data sets (high and low count rates), we found that for the low count rates data the model fitted always becomes insensitive to the additional model component. According to XSPEC manual, this result means that the fit is unable to constrain the parameter and it should be considered indeterminate, which usually indicates that the model is not appropriate. In order to be consistent in comparing the spectral properties of the X-ray emission at different flux levels, we decided to use only single-component models to fit all *Swift/XRT* observations along the decay period of IGR J17091–3624. Under this assumption, we found that an absorbed power-law spectra fits consistently to all *Swift/XRT* observations. From this model, we estimate fluxes in the 0.7–10 keV energy range for the WT mode data[5] and the 0.5–10 keV energy range for the PC mode data. Both the $N_{\rm H}$ and the photon index (Γ) were free to vary during the fitting as this was necessary to compare with the results reported by Wijnands et al. (2015). Data for which the error bars on Γ exceeded 0.5 were discarded. The results are discussed in Sections 4.2 and 5.5.

3.2 *XMM–Newton*/EPIC data

With the *XMM–Newton* observations corresponding to the lowest flux observed from the source during the 2011–2013 outburst decay, we were able to investigate if the source actually reached quiescence by considering the most commonly used models for LMXBs at this stage: BREMSS and POWERLAW spectral shapes. We fitted the three *EPIC* spectra simultaneously, for the 0.5–10 keV energy range, with $N_{\rm H}$ value linked between observations and all the parameters varying freely during the fitting. We used independent normalization parameters for the *MOS* and *pn* CCD cameras. For the BREMSS spectral shape, no good fit was found, the model errors were always above 50 per cent of the estimated value. We obtained the best fit to our data using the absorbed POWERLAW model with $N_{\rm H} = 1.1 \pm 0.2 \times 10^{22}\,{\rm cm}^{-2}$, in excellent agreement with the outburst value reported by Rodriguez et al. (2011) from *Swift/XRT* and *INTEGRAL/ISGRI* data. We estimated an absorbed flux value of $1.4 \pm 0.2 \times 10^{-13}\,{\rm erg\,s^{-1}\,cm^{-2}}$ in the 0.5–10 keV energy band, with a hard photon index $\Gamma = 1.6 \pm 0.1$, consistent with previous findings for the quiet period in 2006–2007 from Wijnands et al. (2012).

[2] http://cxc.harvard.edu/ciao/threads/spectra_hetgacis
[3] http://cxc.harvard.edu/ciao/ahelp/specextract.html
[4] http://cxc.harvard.edu/ciao/ahelp/tgextract2.html
[5] http://www.swift.ac.uk/analysis/xrt/digest_cal.php

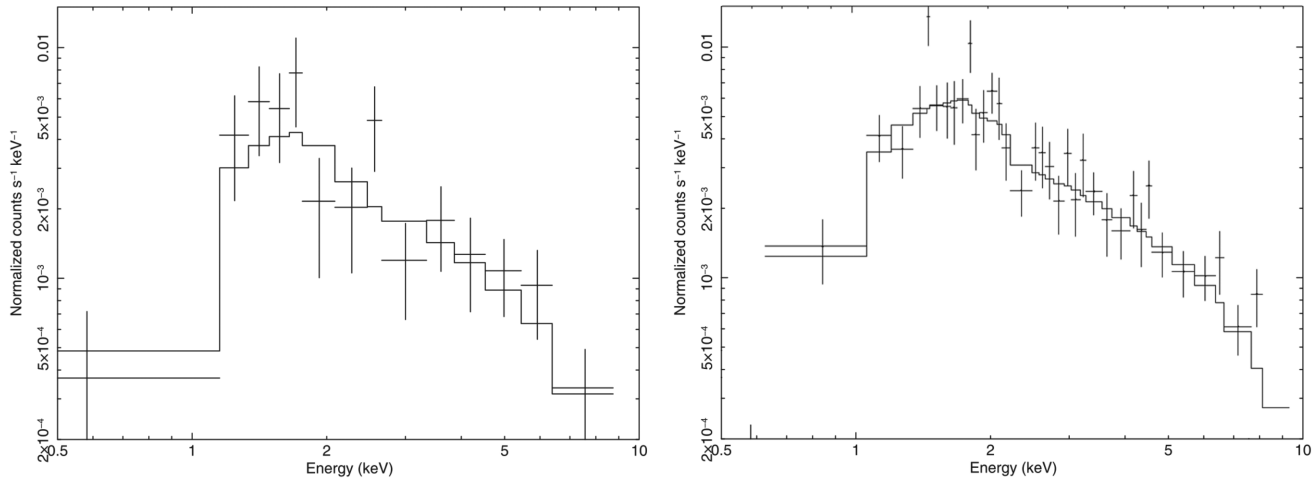

Figure 2. We compare here the *XMM–Newton EPIC/pn* spectrum from Wijnands et al. (2012, left-hand panel) to the *XMM–Newton EPIC/pn* spectrum of IGR J17091–3624 at the low-luminosity period in 2013 (right-hand panel), to illustrate the higher statistics obtained from our data set. The solid line through the data points is the best-fitting absorbed power-law model.

We also used *EPIC* data to investigate the possible contribution of a thermal component to the X-ray spectra, expected to be observed in NS LMXBs in quiescence but not for the case of BH systems (Bildsten & Rutledge 2001). From all observations at the lowest count rates, only *EPIC/pn* data were considered for this attempt given its higher count rates and statistical significance compared to *EPIC/MOS* and *Chandra/HETGS* data sets. For *EPIC/pn* spectra, we added a thermal component to the POWERLAW fitting, considering BBODY, DISKBB, and NSATMOS spectral shapes, independently. Estimated errors were above 50 per cent of the estimated value for the temperature of the thermal component in all cases, likely caused by the fit being insensitive to the parameter. An F-TEST applied to compare POWERLAW with multiple-component models yields a probability value of 0.85, 0.98, and 0.74 for the BBODY + POWERLAW, DISKBB + POWERLAW, and NSATMOS + POWERLAW models, respectively, which indicates that adding an extra model to the fitting does not improve the modeling of the spectra. Similar to our *Swift/XRT* results, for data with the lowest count rates, we conclude that multiple-component models are not appropriate to fit these observations.

3.3 *Chandra/HETGS* data

From each *Chandra* observation, we obtained three different spectra: one zeroth-order spectrum and two more spectra from each arm of the *HETGS* (first order of HEG and MEG). To account for the limited quality of the first-order spectra, we performed a two-step spectral fitting as follows:

(i) We first fit the three *HETGS* zeroth-order spectra simultaneously, considering a POWERLAW model with $N_{\rm H}$ value linked between observations and all the parameters varying freely during the fitting. We obtained an $N_{\rm H} = 1.1 \pm 0.2 \times 10^{22}\,{\rm cm}^{-2}$, consistent with that obtained from *XMM–Newton* observations (our higher quality data).

(ii) To better constrain the photon index values in the models, we add the first-order spectra to the fitting. Given the low count rates of the first-order spectra, we used *cash* statistics to fit the data in this case, fixing $N_{\rm H}$ to $1.1 \times 10^{22}\,{\rm cm}^{-2}$ and fitting simultaneously the three spectra (one zeroth order and two first-order spectra).

(iii) We performed the model fitting for each observation, independently.

The log of the observations for all *Chandra/HETGS* and *XMM–Newton* data sets, as well as the results for the best-fitting model (POWERLAW), are presented in Table 1 and 2.

4 RESULTS

We present the *Swift/XRT* long term X-ray light curve of IGR J17091–3624 from 2011 February to 2018 February in the top panel of Fig. 1. The light curve clearly shows the last two outbursts of the source and the low-luminosity period following the 2011. We also identify four re-brightening events or *re-flares* in the light curve. A zoom in on the light curve is presented at the bottom panel of Fig. 1, showing the transition of IGR 17091–3624 from the 2011 outburst towards the lowest luminosity period of the source in 2013. The green and red lines indicate the times at which *XMM–Newton* and *Chandra* observations were performed, respectively. We used these five observations, one from *XMM–Newton* and four from *Chandra*, to characterize the X-ray emission of IGR 17091–3624 at the lowest count rates observed in 2013.

4.1 Long term evolution

The first *Swift/XRT* detection of IGR J17091–3624 in 2011 corresponds to the outburst onset on February 3 (MJD 55595). After 22 d (MJD 55616), the flux increased to its maximum value and remained approximately constant for the next 245 d, with an average count rate of $\sim$38 counts s^{-1}. Due to Sun constraints from 2011 October 26 (MJD 55860), no observations were performed by *Swift* until after 2012 January 26 (MJD 55952). At this point we observed a steady decrease in the X-ray emission, which reached a minimum count rate of $\sim$1.8 counts s^{-1} on 2012 May 10 (MJD 56057). We identified four re-flares peaking at 2012 June, October and 2013 April, July, corresponding to MJDs 56098, 56225, 56385, and 56478, respectively. Before the 2016 outburst onset, from the last *Swift/XRT* detection of IGR J17091–3624, we estimated the lowest count rate for this source to be $\sim 10^{-2}$ counts s^{-1} in 2013 September 10 (MJD 56545).

In 2016 February 26 (MJD 57444), evidence of renewed activity in IGR J17091–3624 was detected by *Swift/BAT* (Miller et al. 2016), which implies a quiet period of $\sim$900 d. The flux of the source

Table 2. Model fitting results for the low-luminosity period, at 90 per cent level of confidence.

MJD	Obs IDs	Number of spectra fitted	N_H (10^{22} cm^{-2})	Γ	F_{abs}[a] (10^{-13} erg s^{-1} cm^{-2})	F_{unabs}[a] (10^{-13} erg s^{-1} cm^{-2})
			Chandra			
56478	14658	3	Fixed to 1.1	1.2 ± 0.1	25 ± 1	31 ± 1
56509	14659	3	Fixed to 1.1	1.6 ± 0.3	$2.4^{+0.6}_{-0.7}$	$3.5^{+0.5}_{-0.4}$
56558	14660	3	Fixed to 1.1	1.9 ± 0.2	$2.5^{+0.4}_{-0.3}$	4.2 ± 0.5
56591	14661	3	Fixed to 1.1	1.3 ± 0.2	$6.1^{+0.7}_{-0.6}$	$8.0^{+0.7}_{-0.6}$
			XMM–Newton			
56547	0721 200 101	3	1.1	1.6 ± 0.1	1.4 ± 0.2	$2.3^{+0.3}_{-0.6}$

Note.[a]Flux values correspond to the 0.5–10 keV energy band.

Table 3. X-Ray fluxes (0.5–10 keV) estimated for the re-flares. The results are reported at 90-per cent level of confidence. General properties for the two main outburst experienced by the source, before and after the re-flare period, are also listed to add context to the long term evolution.

MJD	Telescope/ Instrument	Notes	F_{unabs} (10^{-10} erg s^{-1} cm^{-2})	Γ	χ^2/d.o.f.
		Main Outburst 2011			
55595	*Swift*/*XRT*	3rd February 2011, outburst onset	2.55 ± 0.20	1.7 ± 0.05	771/795
55616	*Swift*/*XRT*	24th February 2011, outburst maximum flux	22.1 ± 0.20	2.5 ± 0.02	1047/814
55952	*Swift*/*XRT*	January 2012, after sun constraints period	6.92 ± 0.1	2.4 ± 0.02	925/691
56057	*Swift*/*XRT*	May 2012, minimum flux after main outburst	1.44 ± 0.1	2.0 ± 0.10	428/528
		Re-flaring period 2012–2013			
56098	*Swift*/*XRT*	June 2012, first re-flare (peak)	3.50 ± 0.10	1.7 ± 0.04	446/399
56140	*Swift*/*XRT*	August 2012, first re-flare (minimum)	1.06 ± 0.02	1.5 ± 0.10	254/212
56225	*Swift*/*XRT*	October 2012, second re-flare (peak)	3.99 ± 0.25	1.6 ± 0.10	72/55
56320	*Swift*/*XRT*	January 2013, second re-flare (minimum)	0.40 ± 0.04	1.3 ± 0.20	22/19
56385	*Swift*/*XRT*	April 2013, third re-flare (peak)	1.69 ± 0.10	1.5 ± 0.10	51/39
56414	*Swift*/*XRT*	May 2013, third re-flare (minimum)	0.66 ± 0.07	1.2 ± 0.20	30/32
56467	*Swift*/*XRT*	Upper limit from *Swift*/XRT detections in 2013[a]	≤ 0.01	–	
56478	*Chandra*/*HETGS*	July 2013, fourth re-flare (peak)	0.031 ± 0.001	1.2 ± 0.1	54/65
56547	*XMM–Newton*/*EPIC*	September 2013, fourth re-flare (minimum)	$0.0023^{+0.0003}_{-0.0006}$	1.6 ± 0.1	46/46
		Main Outburst 2016			
57444	*Swift*/*XRT*	February 2016, outburst onset	2.25 ± 0.02	1.6 ± 0.03	785/796
57470	*Swift*/*XRT*	March 2016, outburst maximum flux	13.9 ± 0.10	2.2 ± 0.01	1289/872
57610	*Swift*/*XRT*	August 2016, minimum flux after main outburst	0.69 ± 0.02	1.8 ± 0.1	682/695
57640	*Swift*/*XRT*	Upper limit from *Swift*/XRT detections in 2016[a]	≤ 0.01	–	

Note. [a]Upper limits correspond to *Swift*/XRT spectral fitting that yields errors in Γ above 30 per cent of the estimated value.

increased gradually, in the following 26 d, reaching a maximum count rate of $\sim$34 counts s^{-1} on March 23 (MJD 57470). After 2016 May 9 (MJD 57517), the outburst decay period started with a fast decrease in the source flux observed from 2016 May to October (MJD 57517 – 7663), just before the next Sun constrained period. The last *Swift*/*XRT* observation of IGR J17091–3624 was performed on 2018 February 3 (MJD 58152) with $\sim 3.5 \times 10^{-2}$ counts s^{-1}, being the lowest count rate reported for its 2016 outburst.

We found that during the 2011–2013 outburst, the X-ray emission of IGR J17091–3624 remained at a relatively high flux level, above outburst onset value ($\sim 5 \times 10^{-10}$ erg cm^{-2} s^{-1}), for approximately 7.5 times longer than it did in 2016. We estimated similar peak count rates for both outbursts at their highest luminosity period ($\sim$38 counts s^{-1}). However, the flux's decay was steeper in the 2016 outburst. We note that the flare-like behaviour is only observed during the decay of the 2011–2013 outburst, but we are aware that no continuous observations were performed by *Swift*/*XRT* between 2016 October 4 (MJD 57665) and 2018 February 3 2018 (MJD 58152), when the source might have exhibited this variability again. Moreover, the count rate of $\sim$1.8 counts s^{-1} at the beginning of the re-flaring period in the 2011–2013 outburst is two orders of magnitude higher than the lowest count rate observed following the decay period of the 2016 outburst ($\sim 2 \times 10^{-2}$ counts s^{-1}). If any re-flare occurred after the observed decay period of the 2016 outburst, they would have started at significantly lower flux levels ($\sim 4 \times 10^{-12}$ erg cm^{-2} s^{-1} from the last outburst, compared to the $\sim 7 \times 10^{-10}$ erg cm^{-2} s^{-1} of the former). We summarize these results in Table 3.

4.2 Re-flaring activity

For the study of the re-flares properties, whose detailed analysis is out of the scope of this work, we only focus on the periods when the higher and lower count rates were observed for each re-flare independently. We assumed that these periods represent the

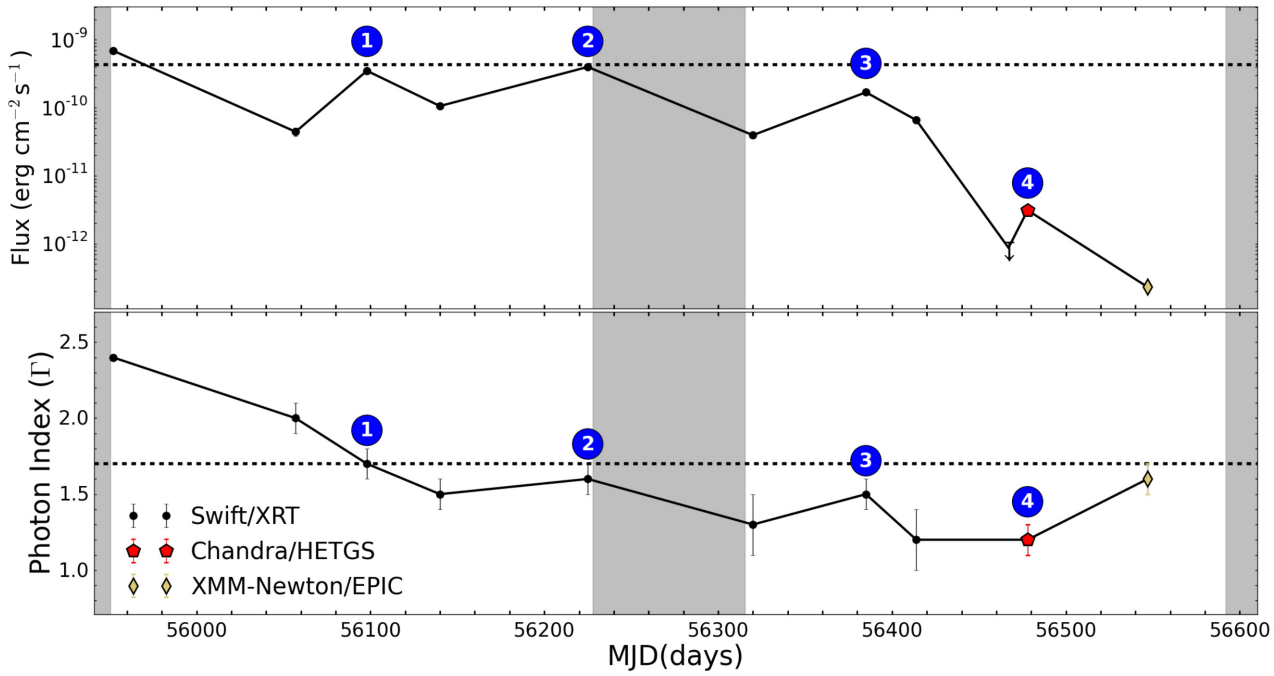

Figure 3. Tail end of the 2011–2013 outburst**.** We present the estimated fluxes (top panel) and photon index values (bottom panel) for IGR J17091–3624 at the last part of its 2011–2013 outburst. *Swift*/XRT, *Chandra*/HETGS, and *XMM–Newton*/EPIC data are marked with black dots, red pentagons and yellow diamonds, respectively. Sun constraints periods are indicated by shaded grey areas. The black arrow marks the upper limit for the flux obtained from *Swift*/XRT spectra with the lowest count rates. The dashed line indicates the flux level (4.3×10^{-10} erg cm^{-2} s^{-1}) and photon index value ($\Gamma = 1.7$) reported by Krimm & Kennea 2011 for the outburst onset in 2011. The flux of the source was found to be always below the outburst onset value along the whole re-flaring period, with no significant evidence of temporal evolution in the spectral shape.

maximum and minimum change in the photon index Γ, or spectral shape, for the corresponding change observed in the X-ray flux of the source as it fades to relative quiescence. In Fig. 3, we present the re-flaring period experienced by IGR J17091–3624 at the tail end of its 2011–2013 outburst, between 2012 May and 2013 October (MJD 55952–56595), using the X-ray fluxes (top panel) and photon index values (bottom panel) obtained from model fitting described in Section 3. We plot and analyse the four re-flares, identified in Fig. 1, by taking the highest and lowest values from the fluxes estimated for each re-flare independently. The data used for this purpose are presented in Table 3. We found the time difference between the peaks of the re-flares (Δt) to be ∼127, ∼160, and ∼93 d. We found no evident periodicity in the occurrence of these re-flares, but we note that the time period between the second and the third re-flare was not properly covered due to a Sun constraint and that four events might be too small a sample to look for a periodicity. We note that during the re-flaring activity, the flux level of IGR J17091–3624 remains always below the value reported by Krimm & Kennea (2011) at the outburst onset in 2011 (indicated by the black dotted line). For the X-ray emission of the source in the 0.5–10 keV band, we found that fluxes on the peaks of the first three re-flares are two orders of magnitude higher than the X-ray flux obtained from the peak of the fourth re-flare. Although changes in the flux level are evident in the light curve, changes in the spectral shape of the X-ray emission are not that clear. We estimated an average photon index value ($\overline{\Gamma}$) for the highest and lowest flux values reached during the four re-flares. We found $\overline{\Gamma} = 1.5 \pm 0.1$ for the peaks, while $\overline{\Gamma} = 1.4 \pm 0.2$ for the lowest fluxes. We conclude that there are not significant changes in the photon index along the re-flare period, despite the observed changes in flux seen on each re-flare.

4.3 The low-luminosity period

After the third re-flare, the X-ray emission of the source dropped significantly and *Swift/XRT* spectral modelling only yields an upper limit for the flux of the source. Once the X-ray flux increased during the fourth re-flare, it was possible to model the spectra with a POWERLAW model. However, the errors on the values obtained were large (above 30 per cent of the estimated value, with errors in $\Gamma \geq 0.5$) and therefore we decided to exclude these data (all observations in the period MJDs 56420–56570) from our spectral analysis.

We instead analysed four *Chandra/HETGS* and one *XMM–Newton/EPIC* observations that were performed with higher sensitivity in the same period of time. The data cover a five-month period, between 2013 June and October (MJD 56477–56592), 2.2 yr after the 2011–2013 outburst onset in 2011 February and 2.3 yr before the source renewed outburst activity in 2016 February. We present in Fig. 4 the temporal evolution of the X-ray emission of the source during this period. *Chandra* and *XMM–Newton* observations are labelled in red and green, respectively. In order to put our results in the context of previous findings, we indicate with a purple dashed line the lowest flux level and photon index value reported by Wijnands et al. (2012) for the previous low-luminosity period of the source observed in 2006 and 2007 ($9 \pm 5 \times 10^{-14}$ erg s^{-1} cm^{-2}, $\Gamma = 1.6 \pm 0.5$). In the top panel, we present our flux estimates, showing the peak of the fourth re-flare experienced by IGR J17091–3624 at MJD 56478 (2013 July 5), and the subsequent decay of its X-ray emission. From the *Chandra* observation performed on MJD 56478, at the peak of the fourth re-flare, we estimated a flux value of $\sim 3.1 \times 10^{-12}$ erg s^{-1} cm^{-2}. In the following 70 d, the flux decreases by a factor of 10, when the source reached its lowest observed flux

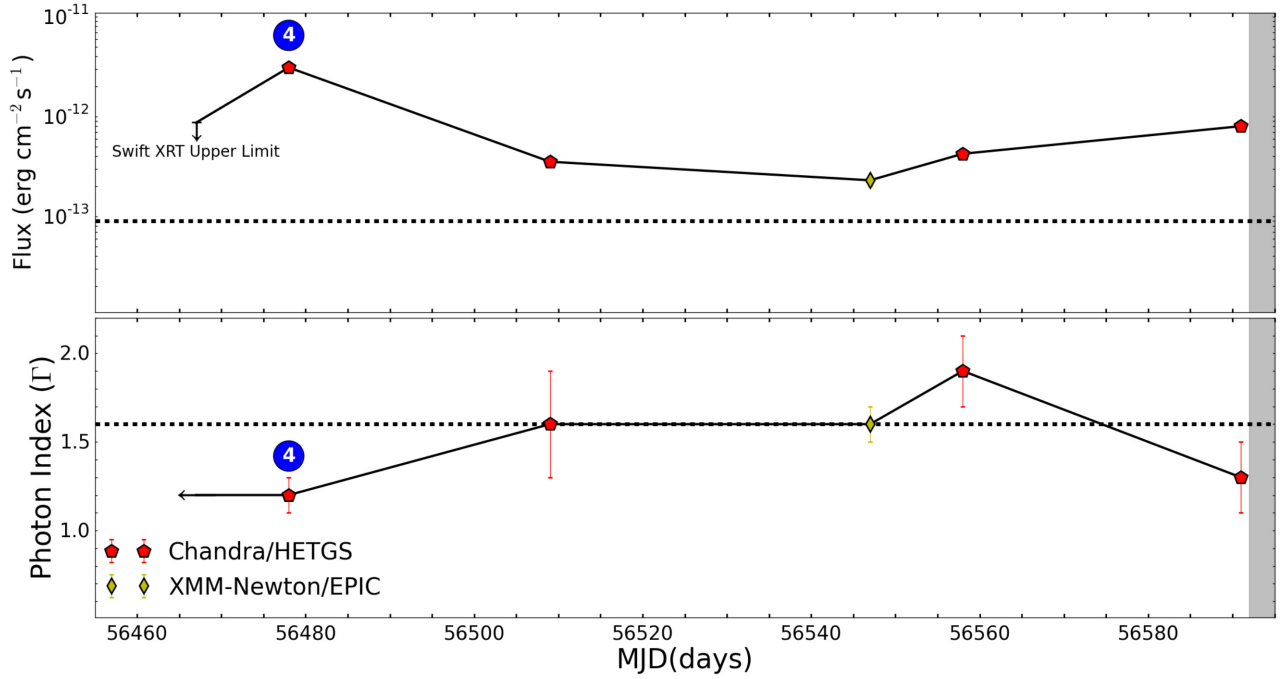

Figure 4. The low-luminosity period**.** We present the estimated fluxes (top panel) and photon index values (bottom panel) for IGR J17091–3624 at the very end of its 2011–2013 outburst. *Swift*/*XRT*, *Chandra*/*HETGS*, and *XMM–Newton*/*EPIC* data are marked with black dots, red pentagons, and yellow diamonds, respectively. Sun constraints periods are indicated by shaded grey areas. Black arrows mark the upper limits from *Swift*/*XRT* detections. The dashed lines indicate the flux level ($9 \pm 5 \times 10^{-14}$ erg cm^{-2} s^{-1}) and photon index value ($\Gamma = 1.6$) reported by Wijnands et al. (2012) for the previous quiescent period of the source in 2006. Slight variability is observed in the X-ray flux, but we did not find strong evidence of softening in the spectra.

on 2013 September, with a value of $\sim 0.23 \times 10^{-12}$ erg s^{-1} cm^{-2} in the 0.5–10 keV band. In the following 40 d the flux of the source increased again, this time only by a factor of 5, as seen by the last *Chandra* observations before the Sun constrained period started in 2013 October. Since no observations were available after MJD 56600, we cannot discard the possibility that the observed increase in the flux is related to a new re-flare happening at the very end of the 2011–2013 outburst.

The corresponding photon index values obtained from these five observations are shown in the bottom panel of Fig. 4. Although we observed a factor of 5–10 change in the flux levels, corresponding changes in the photon index are not evident. We investigated the statistical significance of this result by performing an F-test to the spectral fitting. To guarantee a statistically meaningful F-test, we only considered the data sets with highest quality: *XMM–Newton*/*EPIC*/*pn* and *Chandra*/*HETGS*/zeroth-order. We fitted the five spectra simultaneously, using a single component POWERLAW model with the photon index varying freely, fixed $N_{\rm H} = 1.1$ and free normalization parameters to allow differences in the flux level. If the photon index is set to vary freely, but tied between observations, we obtain a constant photon index value of $\sim 1.4 \pm 0.1$ with χ^2/d.o.f = 145.53/144. When we set the photon index to vary independently per observation, we obtain different photon index values (see Table 2) and a χ^2/d.o.f of 121.28/140. We then apply an F−test on these results and obtain a probability value of 3.9×10^{-5}, suggesting that the spectral shape does not remain constant as the source fades into quiescence. However, we found no evidence of a systematic softening of the spectra. The $\Gamma = 1.6 \pm 0.1$ obtained for the lowest flux observed in the low-luminosity period is consistent to the mean value estimated for the re-flares ($\overline{\Gamma} = 1.45 \pm 0.15$) at higher luminosities. It is interesting to note that spectral softening in the spectra of LMXBs is expected at low luminosities, regardless of the nature of its compact object. For the BH systems, the softening seems to level off at a photon index $\sim$2, while the NSs reach photon indices of 2.5–3 (Plotkin et al. 2013; Wijnands et al. 2015). The relatively hard spectra we found in the case of IGR J17091–3624, even at its lowest luminosities, might favour the idea that the source did not reach true quiescence in 2013.

5 DISCUSSION

5.1 Outbursts properties

During the last two outbursts, the source's X-ray flux reached similar maximum values but we found two main differences between them:

(i) *Time-scales*: The high flux levels in the 2011–2013 outburst lasted longer than those in 2016. The decay of the X-ray emission to the lowest count rates at the tail end of each outburst was slower for the former.

(ii) *Re-flaring*: Re-flares are clearly identified in the long-term light curve for the 2011–2013 outburst. Three re-flares occurred during the decay of the source's emission towards lower count rates and a fourth re-flare was observed even at its lowest luminosities, while no such re-flaring was detected in the 2016 outburst.

We note that there are no observations from *Swift*/*XRT* after 2016 November and we cannot rule out that the source shows re-flaring afterwards. Given that the flux level at the end of the 2016 outburst is approximately two orders of magnitude lower than the flux observed at the beginning of the re-flare period in 2011–2013, we conclude that any subsequent re-flaring activity in 2016 would be weaker than the one observed in the former outburst. Moreover, it has been shown

by some authors that many X-ray transients show different outburst profiles and that re-flare events are not necessarily active after each outburst in LMXBs (Parikh et al. 2017; Capitanio et al. 2015). In this context, the absence of re-flares after the 2016 outburst would not be an unusual behaviour for an LMXB like IGR J17091–3624 either.

5.2 The re-flaring activity

What makes the re-flaring activity in LMXBs still puzzling nowadays is that recent studies show that several sources do actually transit from hard to soft states and back during the re-flares (e.g. MAXI J1535–571 and GRS 1739–278; Yan & Yu 2017; Parikh et al. 2019; Cúneo et al. 2020). For these sources, it's been argued that the transition hard-to-soft/soft-to-hard during the re-flare would depend on the transition luminosity of the main outburst. Only when the luminosity at the re-flare reaches the level at which the hard-to-soft transition happened for the main outburst, the source will transit to the soft state during the re-flare, otherwise it will not. In Fig. 3, we showed that the flux obtained for the re-flares of IGR J17091–3624 never went above the flux level reported for the outburst onset, which is actually below the flux level of the hard-to-soft transition (Krimm & Kennea 2011; Shaposhnikov 2011). This might explain why the source did not transit back to the soft state, showing no change in the photon index values, in any of the re-flares. We are aware that simultaneous and quasi-simultaneous X-Ray and radio/NIR/optical/UV follow up of IGR J17091–3624 re-flares are needed to better constraint their properties, but this analysis is out of the scope of this work.

5.3 Black hole or neutron star system

To accurately distinguish between a BH and an NS, LMXB often requires direct measurements of the physical properties of the compact object such as orbital parameters, masses, and, when possible, to probe the existence of an event horizon or star's surface. Unambiguous observational probes that serve to this purpose are: (i)– thermonuclear bursts and pulsations (only observed in NSs, Strohmayer & Bildsten 2006; Galloway et al. 2008, and references therein), and (ii)– mass estimates based on radial velocity measurements (for NS, $M_\star \leq 3\,M_\odot$ and $M_\star \geq 3\,M_\odot$ for BH systems). In the particular case of IGR J17091–3624, no thermonuclear bursts or pulsations are observed in its light curves and no direct measurement of its mass has been reported so far. The fact that its variability in outburst resembles the one observed in the BH GRS 1915+105 has been often accepted as strong evidence to classify it as a BH LMXB. However, the NS source MXB 1730–335 has also shown similar X-ray variability (Bagnoli & in't Zand 2015), probing that this kind of variability is unrelated to the nature of the accretor. The similarities with GRS 1915+105 have been used in previous works to constrain the mass of compact object inside IGR J17091–3624, but while some authors place the mass of the system very close to the NS regime ($M \leq 5\,M_\odot$, see e.g. Altamirano et al. 2011 and Rao & Vadawale 2012) other studies favour the BH scenario by suggesting a higher mass for this source (between 8.7 and 15.6 $M_\odot$, Altamirano & Belloni 2012; Rebusco et al. 2012; Iyer, Nandi & Mandal 2015). To further investigate the nature of the accretor in IGR J17091–3624, we considered the possible contribution of a thermal component in the X-ray spectra. Assuming that IGR J17091–3624 hosts an NS, we can analyse its X-ray emission at low luminosities to account for the thermal emission associated to the NS surface. Since we have stated in Section 3.2 that multi-component models are not well constrainted due to the lowest count rates in our spectra, it is only possible to estimate an upper limit for the NS temperature. We considered canonical values for the NS ($M_{\rm NS} = 1.4\,M_\odot$, $R_{\rm NS} = 10$ km) and the normalization fixed to unity, with the temperature as the only free parameter during the fitting. For $D = 8$ and 35 kpc, we obtained an upper limit for the NS temperature (as seen by an observer at infinity) of $kT_{\rm eff}^{\infty} \sim 68$ and 136 eV, respectively. It is interesting to note that a value of $kT \sim 136$ eV would be, in fact, very consistent with the temperature reported for the NS SAX J17508–2900 when this source developed post-outburst 'rebrightenings', similar to those observed in IGR J17091–3624, after its 2008 outburst (Parikh & Wijnands 2017). If this hot thermal component is confirmed, our results would place IGR J17091–3624 among the hottest known NSs and rather peculiar. Although the detection of a thermal contribution in the spectra of LMXBs at their lowest luminosities could be attributed to the NS nature of the accretor, some studies have shown that for several NS systems such as SAX J1808.4–3658 and EXO 1745–248, the X-ray spectra in quiescence are well described with a pure power-law spectrum. These results would necessarily imply that probing the non-existence of a thermal component might not be enough to exclude an NS system inside IGR J17091–3624 (see e.g. discussion in Degenaar & Wijnands 2012).

5.4 The true quiescent state

To investigate this, we can start by assuming that the lowest fluxes observed do correspond to the quiescent state of IGR J17091–3624, estimate its quiescent X-ray luminosity ($L_{\rm q}$) and compare it with the known distribution of BHs and NSs luminosities in quiescence. Since the distance to IGR J17091–3624 is still unknown, we considered the wide range of distances found in the literature (e.g. Rodriguez et al. 2011; Capitanio et al. 2012; Wijnands et al. 2012; Janiuk et al. 2015). We estimated $L_{\rm q}$ ranging between 1.7–4.6 $\times$ 10^{33} and 1.1–3.4 $\times$ 10^{34} erg s^{-1} for distances of 8–13 and 20–35 kpc, respectively. In Fig. 5, we show the X-ray luminosity ($L_{\rm x}$) versus orbital period ($P_{\rm orb}$) of confirmed NS and BH systems at quiescence, taken from Reynolds & Miller (2011). NS and BH systems are plotted with blue and black symbols, respectively. We mark the upper and lower limits with arrows. Based on our estimated $L_{\rm q}$, we indicate the approximate location of IGR J17091–3624 within this diagram. Given that no orbital period has been determined for IGR J17091–3624, we use a horizontal green strip (at the top of the figure) to compare the source with the known NS and BH binaries. If IGR J17091–3624 was in true quiescence at this time, our results would place the source among the few BH LMXBs with significantly high $L_{\rm q}$. These findings are consistent with those reported by Wijnands et al. (2012), which pointed out that the high luminosity obtained would entail an orbital period $\geq$200 h for IGR J17091–3624. They argue that such a long orbital period would favour the BH nature of the binary system, given the orbital period observed in GRS 1915+105. Their results also suggest that the high luminosity found for IGR J17091–3624 could imply that the source has not reached true quiescence at the time of the observations in 2006–2007. Similar results are found when we compare IGR J17091–3624 with the NS LMXBs population. The estimated $L_{\rm q}$ would place IGR J17091–3624 also among the few NS sources, such as EXO 0748–676 (the blue star in the green shaded area), with relatively high luminosity in quiescence. Although, based on the evidence of residual accretion in quiescence provided by Díaz Trigo et al. (2011) and peculiarities pointed out by Degenaar et al. (2011), EXO 0748–676 seems to be more an exception than the rule. Irrespective of the accretor inside IGR J17091–3624, an estimate of the normalized Eddington luminosity for distances $D = 8$–35 kpc yields $l_{\rm x} = 10^{-6}$ to 10^{-5} (as defined by Plotkin et al. 2013 and with $M = 8$–16 $M_\odot$ taken from Iyer et al. 2015), which is just above

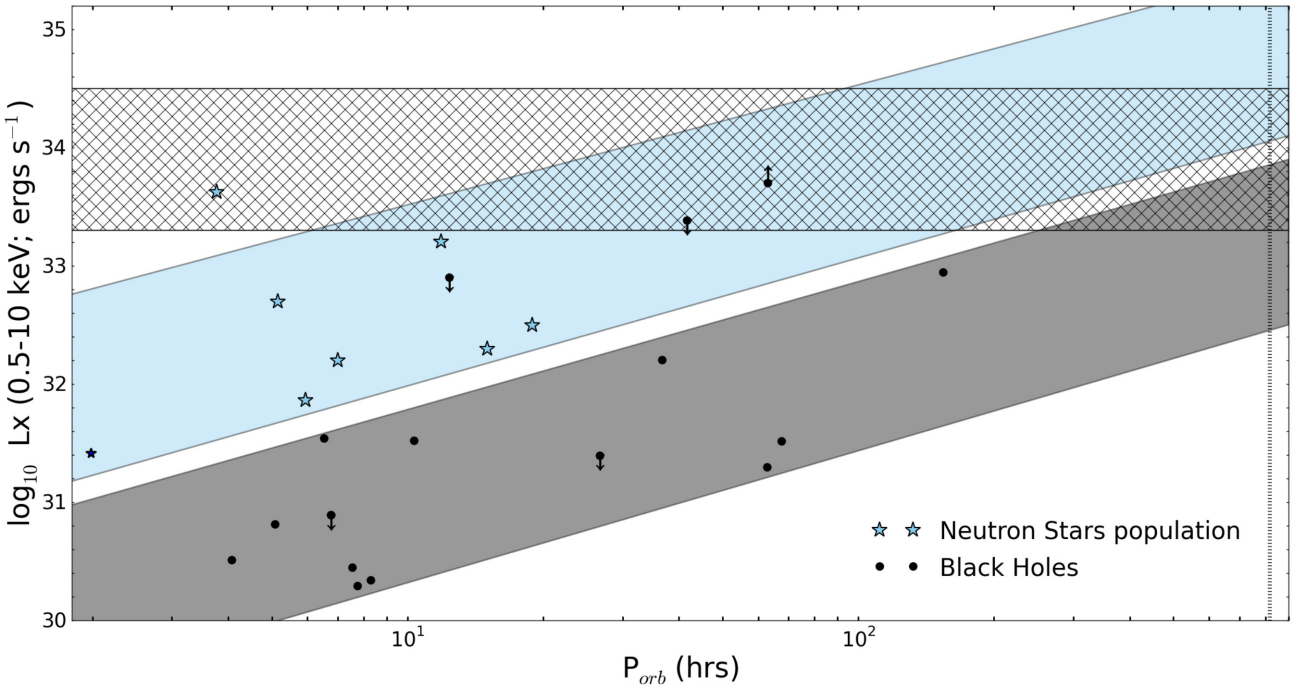

Figure 5. L_x versus P_{orb} for confirmed NS (blue stars) and BH (black dots) binaries. Gray and blue shaded areas mark the expected distribution for these two populations within this diagram, according to Reynolds & Miller (2011). We marked with a hatched region the approximate location of IGR J17091–3624. The orbital period of GRS 1915+105 is also indicated, close to the right-hand edge of the plot, with a dotted vertical line.

the upper limit value expected for the quiescent state ($l_x \sim 10^{-5.5}$). Therefore, it is highly likely that we have not seen the source at its true quiescent state so far.

5.5 Spectral evolution with X-ray luminosity

The analysis of the X-ray emission of different NS and BH binaries demonstrated that, irrespective of the nature of the compact object, their spectra seem to become softer with decreasing luminosities (see e.g. Plotkin et al. 2013; Reynolds et al. 2014). Moreover, Wijnands et al. (2015) suggested that there is a clear difference in spectral properties of the global population of BH and NS systems at luminosities below 10^{35} erg s^{-1}. In Fig. 6, we present the photon index (Γ) and corresponding X-ray luminosity (L_x) for different LMXBs taken from Wijnands et al. (2015). A strong correlation between decreasing luminosity and softening of the spectra is observed in both types of LMXBs. But, while the spectra from NS systems become softer at relatively high luminosities, $\sim 10^{36}$ erg s^{-1}, for the BHs systems, softening is only seen after they reach luminosities below 10^{34} erg s^{-1}. Additionally, the photon index values in the case of BH binaries seem to plateau around $\Gamma \sim 2.0$ towards quiescence state (Plotkin et al. 2013), whereas higher Γ values are found in the case of NS systems. To analyse the behaviour of IGR J17091–3624 in the context of the whole population of LMXBs, we have plotted in green squares the corresponding L_x and Γ obtained from *Swift*/*XRT*, *XMM–Newton*, and *Chandra* data for distances of 8 kpc (top panel) and 35 kpc (bottom panel), respectively. In the high L_x regime, above $\sim 10^{36}$ erg s^{-1}, our results nicely trace a hysteresis loop with the corresponding transitions from hard-to-soft and soft-to-hard states for the outbursts of the source in 2011 (open symbols) and 2016 (filled symbols). It is also seen from this plot that, below $L_x = \sim 10^{36}$ erg s^{-1}, IGR J17091–3624 luminosity drops by two orders of magnitude but its spectra never become softer than 1.7. Under the assumption that softening in the spectra of NS binaries is expected to occur at luminosities below 10^{36} erg s^{-1}, we conclude the following:

(i) For IGR J17091–3624 located at a distance of 8 kpc (top panel), the source reached L_x as 10^{33} erg s^{-1} with no evidence of softening in the spectra, which would rule out an NS nature for the accretor. None the less, the photon index found for IGR J17091–3624 is slightly harder than the expected values for a BH source.

(ii) If the source is located at larger distances (bottom panel, at $D = 35$ kpc), the observed trend seems to be better match the values found for the BH population rather than that of the NS systems.

6 CONCLUDING REMARKS

We presented a general description of the X-ray emission of IGR J17091–3624 during the past 10 yr as seen by *Swift*/*XRT*, *Chandra*, and *XMM–Newton*. We clearly identified the 2011–2013 outburst showing flare-like behaviour and characterized the low level variability observed from 2013 June to October at a flux level below 5×10^{-10} erg cm^{-2} s^{-1}. We observed that the source reached the same flux level at the tail end of the 2016 outburst but showed no variability of any kind. Based on the analysis of the long term *Swift*/*XRT* light curve, we found that the last two outbursts of IGR J17091–3624 evolved on different time-scales. Using *XMM–Newton* and *Chandra* data, we found that the X-ray flux from the source changes by a factor of ∼5–10 at its low-luminosity period in 2013, but we did not find strong evidence of spectral softening at this stage which might imply the source has not been observed in its true quiescent state so far. We compared the spectral properties of IGR J17091–3624, during its transition to quiescence, with the spectral behaviour observed in the whole population of LMXBs, and conclude that the accretor inside this object seems to behave more like a BH source rather than an NS.

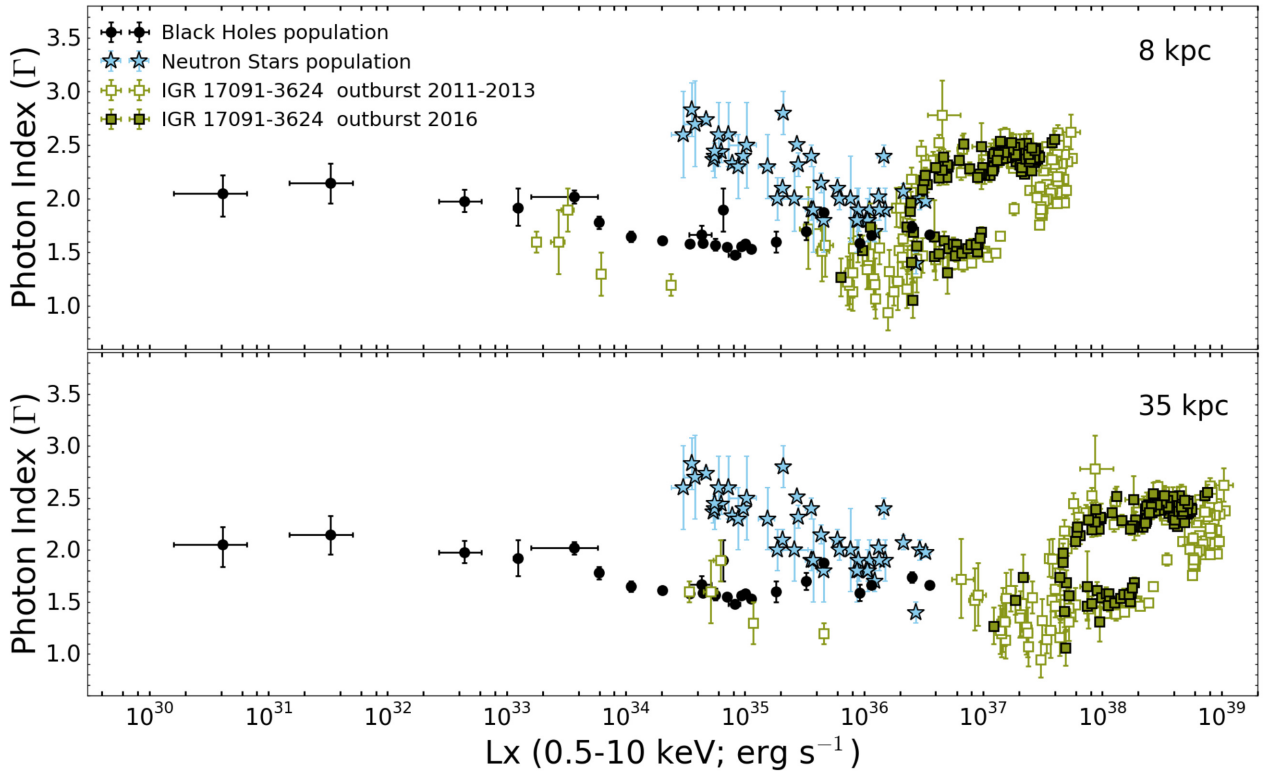

Figure 6. Spectral evolution of LMXBs with decreasing luminosity. Photon index and X-ray luminosities for BHs (black dots) and NS (blue stars) systems taken from Wijnands et al. (2015). The squares in green indicate the luminosity and photon index values obtained for IGR J17091–3624 at its last two outbursts. We present in the top panel the luminosity values obtained considering $d = 8$ kpc and at the bottom panel, the values obtained when we assumed $d = 35$ kpc.

ACKNOWLEDGEMENTS

We thank the anonymous referee for a thorough reading of the manuscript and helpful comments that led to notable improvements in the quality of this work. MP is a faculty for the Future Alumnae of Schlumberger Foundation. She appreciates the financial support from Schlumberger Foundation, the COSPAR Capacity Buil ding Workshops Fellowship Programs, and CONACYT for current funding in the process of publishing this work. DA acknowledges support from the Royal Society. DA and VAC acknowledge support from the Royal Society International Exchanges 'The first step for High-Energy Astrophysics relations between Argentina and UK'. VAC also acknowledges support from the Spanish *Ministerio de Ciencia e Innovación* under grant AYA2017-83216-P. JC thanks the Science & Technology Facilities Council and the Royal Astronomical Society for their financial support. ND is supported by a Vidi grant from the Netherlands Organization for Scientific Research (NWO). AP and RW are supported by an NWO Top Grant, Module 1, awarded to RW. This work made use of data supplied by the UK Swift Science Data Centre at the University of Leicester. We thank the Chandra Help Desk team for their guidance and suggestions using the data reduction and analysis software.

DATA AVAILABILITY

The data sets underlying this article are available in the domain: https://heasarc.gsfc.nasa.gov

REFERENCES

Altamirano D., Belloni T., 2012, ApJ, 747, L4
Altamirano D. et al., 2011, ApJ, 742, L17
Aoki M. et al., 2020, ATel, 13652, 1
Arnaud K. A., 1996, in Jacoby G. H., Barnes J., eds, ASP Conf. Ser. Vol. 101, Astronomical Data Analysis Software and Systems V. Astron. Soc. Pac., San Francisco, p. 17
Bagnoli T., in't Zand J. J. M., 2015, MNRAS, 450, L52
Balakrishnan M., Tetarenko B., Corrales L., Reynolds M., Miller J. M., 2019, ATel, 12848, 1
Barré H., Nye H., Janin G., 1999, ESABu, 100, 15
Belloni T., Klein-Wolt. M., Méndez M., van der Klis M., van Paradijs J., 2000, A&A, 355, 271
Bildsten L., Rutledge R. E., 2001, Kouveliotou C., Ventura J., Heuvel E. V. d., eds, Proc. NATO ASI Conf. Ser Vol. 567, The Neutron Star – Black Hole Connection. Kluwer, Dordrecht, p. 245
Burrows D. N. et al., 2000, Flanagan K. A., Siegmund O. H., eds, SPIE Conf. Ser. Vol. 4140, X-Ray and Gamma-Ray Instrumentation for Astronomy XI. SPIE, Bellingham, p. 64
Capitanio F. et al., 2006, ApJ, 643, 376
Capitanio F., Del Santo M., Bozzo E., Ferrigno C., De Cesare G., Paizis A., 2012, MNRAS, 422, 3130
Capitanio F., Campana R., De Cesare G., Ferrigno C., 2015, MNRAS, 450, 3840
Castro-Tirado A. J., Brandt S., Lundt N., 1992, IAU Circ., 5590, 2
Christodoulou D. M., Laycock S. G. T., Kazanas D., Contopoulos I., 2018, RAA, 18, 142
Court J. M. C., Altamirano D., Pereyra M., Boon C. M., Yamaoka K., Belloni T., Wijnands R., Pahari M., 2017, MNRAS, 468, 4748
Cúneo V. A. et al., 2020, MNRAS, 496, 1001

Degenaar N., Wijnands R., 2012, MNRAS, 422, 581
Degenaar N. et al., 2011, MNRAS, 412, 1409
Díaz Trigo M., Boirin L., Costantini E., Méndez M., Parmar A., 2011, A&A, 528, A150
Evans P. A. et al., 2007, A&A, 469, 379
Evans P. A. et al., 2009, MNRAS, 397, 1177
Fender R. P., Gallo E., Jonker P. G., 2003, MNRAS, 343, L99
Gallo E., Fender R. P., Miller-Jones J. C. A., Merloni A., Jonker P. G., Heinz S., Maccarone T. J., van der Klis M., 2006, MNRAS, 370, 1351
Galloway D. K., Muno M. P., Hartman J. M., Psaltis D., Chakrabarty D., 2008, ApJS, 179, 360
Garmire G. P., Bautz M. W., Ford P. G., Nousek J. A., Ricker G. R., 2003, Truemper J. E., Tananbaum H. D., eds, SPIE Conf. Ser. Vol. 4851, X-Ray and Gamma-Ray Telescopes and Instruments for Astronomy. SPIE, Bellingham. p. 28
Gatuzz E., Díaz Trigo M., Miller-Jones J. C. A., Migliari S., 2020, MNRAS, 491, 4857
Gehrels N. et al., 2004, ApJ, 611, 1005
Grinberg V. et al., 2016, ATel, 8761
Heinke C. O., Deloye C. J., Jonker P. G., Taam R. E., Wijnands R., 2008, AIP Conf. Proc. Vol. 983, 40 Years of Pulsars: Millisecond Pulsars, Magnetars and More. AIP, New York, p. 526
Homan J., Neilsen J., Steiner J., Remillard R., Altamirano D., Gendreau K., Arzoumanian Z., 2019, ATel, 12742, 1
Iyer N., Nandi A., Mandal S., 2015, ApJ, 807, 108
Janiuk A., Czerny B., Siemiginowska A., 2000, ApJ, 542, L33
Janiuk A., Grzedzielski M., Capitanio F., Bianchi S., 2015, A&A, 574, A92
Jonker P. G., Bassa C. G., Wachter S., 2007, MNRAS, 377, 1295
King A. L. et al., 2012, ApJ, 746, L20
Koljonen K., Vera R., Lahteenmaki A., Tornikoski M., 2019, ATel, 12839, 1
Krimm H. A., Kennea J. A., 2011, ATel, 3148, 1
Lasota J.-P., 2001, New Astron. Rev., 45, 449
Lepingwell V. A. et al., 2020, ATel, 13676, 1
Maselli A., Capitanio F., Feroci M., Massa F., Massaro E., Mineo T., 2018, A&A, 612, A33
Miller-Jones J. C. A., Gallo E., Rupen M. P., Mioduszewski A. J., Brisken W., Fender R. P., Jonker P. G., Maccarone T. J., 2008, MNRAS, 388, 1751
Miller-Jones J. C. A., Jonker P. G., Maccarone T. J., Nelemans G., Calvelo D. E., 2011, ApJ, 739, L18
Miller J. M., Reynolds M., Kennea J., King A. L., Tomsick J., 2016, ATel, 8742, 1
Narayan R., McClintock J. E., 2008, New Astron. Rev., 51, 733
Narayan R., Yi I., 1994, ApJ, 428, L13
Negoro H. et al., 2018, ATel, 11828, 1
Pahari M., Misra R., Mukherjee A., Yadav J. S., Pandey S. K., 2013, MNRAS, 436, 2334
Parikh A. S., Wijnands R., 2017, MNRAS, 472, 2742
Parikh A. S., Wijnands R., Degenaar N., Altamirano D., Patruno A., Gusinskaia N. V., Hessels J. W. T., 2017, MNRAS, 468, 3979
Parikh A. S., Russell T. D., Wijnands R., Miller-Jones J. C. A., Sivakoff G. R., Tetarenko A. J., 2019, ApJ, 878, L28
Patruno A., Rea N., Altamirano D., Linares M., Wijnands R., Van Der Klis M., 2009, MNRAS, 396, L51
Patruno A., Maitra D., Curran P. A., D'Angelo C., Fridriksson J. K., Russell D. M., Middleton M., Wijnands R., 2016, ApJ, 817, 100
Plotkin R. M., Gallo E., Jonker P. G., 2013, ApJ, 773, 59
Plotkin R. M. et al., 2016, MNRAS, 456, 2707
Radhika D., Sreehari H., Nandi A., Iyer N., Mandal S., 2018, Ap&SS, 363, 189
Rao A., Vadawale S. V., 2012, ApJ, 757, L12
Rebusco P., Moskalik P., Kluźniak W., Abramowicz M. A., 2012, A&A, 540, L4
Remillard R. A., McClintock J. E., 2006, ARA&A, 44, 49
Revnivtsev M., Chernyakova M., Capitanio F., Westergaard N. J., Shoenfelder V., Gehrels N., Winkler C., 2003, ATel, 132
Reynolds M. T., Miller J. M., 2011, ApJ, 734, L17
Reynolds M. T., Reis R. C., Miller J. M., Cackett C. M., Degenaar N., 2014, MNRAS, 441, 3656
Ridnaia A. et al., 2019, ATel, 13316, 1
Rodriguez J., Corbel S., Caballero I., Tomsick J. A., Tzioumis T., Paizis A., Cadolle Bel M., Kuulkers E., 2011, A&A, 533, L4
Shaposhnikov N., 2011, ATel, 3179, 1
Strohmayer T., Bildsten L., 2006, Compact stellar X-ray sources. Cambridge Univ. Press, Cambridge, p. 113
Strüder L. et al., 2001, A&A, 365, L18
Turner M. J. L. et al., 2001, A&A, 365, L27
Verner D. A., Ferland G. J., Korista K. T., Yakovlev D. G., 1996, ApJ, 465, 487
Weisskopf M. C., 1999, AAS, 195, 96.01
Wijnands R., Degenaar N., 2013, MNRAS, 434, 1599
Wijnands R., Yang Y. J., Altamirano D., 2012, MNRAS, 422, L91
Wijnands R., Degenaar N., Page D., 2013, MNRAS, 432, 2366
Wijnands R., Degenaar N., Armas Padilla M., Altamirano D., Cavecchi Y., Linares M., Bahramian A., Heinke C. O., 2015, MNRAS, 454, 1371
Wilms J., Allen A., McCray R., 2000, ApJ, 542, 914
Xu Y. et al., 2017, ApJ, 851, 103
Yan Z., Yu W., 2017, MNRAS, 470, 4298
Yang Q.-X., 2016, RAA, 16, 62
Zhang Z., Qu J. L., Gao H. Q., Zhang S., Bu Q. C., Ge M. Y., Chen L., Li Z. B., 2014, A&A, 569, A33

This paper has been typeset from a TEX/LATEX file prepared by the author.